Contribution of hydrophobic and electrostatic interactions to the membrane integration of the Shaker K^+ channel voltage sensor domain

Liyan Zhang*, Yoko Sato†, Tara Hessa†, Gunnar von Heijne†, Jong-Kook Lee‡, Itsuo Kodama‡, Masao Sakaguchi§, and Nobuyuki Uozumi*¶‖

¶Department of Biomolecular Engineering, Graduate School of Engineering, Tohoku University, Aobayama 6-6-07, Sendai 980-8579, Japan; *Bioscience and Biotechnology Center, Nagoya University, Nagoya 464-8601, Japan; †Center for Biomembrane Research, Department of Biochemistry and Biophysics, Stockholm University, SE-106 91 Stockholm, Sweden; ‡Research Institute of Environmental Medicine, Nagoya University, Nagoya 464-8601, Japan; and §Graduate School of Life Science, University of Hyogo, Ako Hyogo 678-1297, Japan

Edited by Lily Y. Jan, University of California School of Medicine, San Francisco, CA, and approved March 28, 2007 (received for review December 12, 2006)

Membrane-embedded voltage-sensor domains in voltage-dependent potassium channels (K_v channels) contain an impressive number of charged residues. How can such highly charged protein domains be efficiently inserted into biological membranes? In the plant K_v channel KAT1, the S2, S3, and S4 transmembrane helices insert cooperatively, because the S3, S4, and S3–S4 segments do not have any membrane insertion ability by themselves. Here we show that, in the *Drosophila* Shaker K_v channel, which has a more hydrophobic S3 helix than KAT1, S3 can both insert into the membrane by itself and mediate the insertion of the S3–S4 segment in the absence of S2. An engineered KAT1 S3–S4 segment in which the hydrophobicity of S3 was increased or where S3 was replaced by Shaker S3 behaves as Shaker S3–S4. Electrostatic interactions among charged residues in S2, S3, and S4, including the salt bridges between E283 or E293 in S2 and R368 in S4, are required for fully efficient membrane insertion of the Shaker voltage-sensor domain. These results suggest that cooperative insertion of the voltage-sensor transmembrane helices is a property common to K_v channels and that the degree of cooperativity depends on a balance between electrostatic and hydrophobic forces.

charged residue | K_v channel | salt bridge | translocation

Voltage-dependent K^+ (K_v) channels are found in bacteria, plants and animals. K_v channels are integral membrane proteins with an ion-selective pore domain (S5–P–S6) and a voltage-sensor domain (S1–S4) (1). The voltage-sensor domain contains two and one conserved negatively charged residues in the S2 and S3 transmembrane (TM) helices, respectively, and four or more conserved positively charged residues in S4. The roles of these charged residues in voltage gating have been extensively studied. Several structural models of K_v channels have been proposed on the basis of experimental data and crystal structures (2–14).

An integral membrane protein inserts into the membrane via a translocon, which forms an aqueous channel that permits the translocation of hydrophilic loops and opens laterally to allow the exit of hydrophobic TM helices into the lipid bilayer (15). This process is regulated by topogenic signals in the amino acid sequence that define the final membrane topology (16). In the simplest case the TM helices are integrated into the membrane one by one (17), but in some cases two or more TM helices in the nascent polypeptide need to interact to be able to insert efficiently (18, 19). There have been several studies on the biogenesis of K_v channels (20–25), but these studies have arrived at different results, in particular as regards insertion of the voltage sensor. Our studies on the topogenesis of the plant hyperpolarization-activated, inwardly rectifying channel KAT1 revealed that neither S3 nor S4 can integrate into the membrane independently, whereas, in the presence of S2, S3–S4 can integrate into membrane in a concerted or "posttranslational" manner; charged residues in S2, S3, and S4 are involved in the process (26, 27). However, the question of whether the membrane integration of S3–S4 of other K_v channels occurs by the same mechanism remains to be addressed.

Shaker is a well characterized depolarization-activated, outwardly rectifying K_v channel cloned from *Drosophila* neurons (28, 29). The Shaker S3 and S4 TMs have a higher hydrophobicity than those of KAT1 S3 and S4 [Fig. 5*A* and supporting information (SI) Fig. 8], leading us to suspect that the mechanism of membrane insertion of the Shaker voltage-sensor domain may differ from that previously reported for KAT1 (26, 27). The present study was designed to systematically examine the membrane integration of Shaker and to test the generality of the proposed integration mechanism for voltage-sensor domains.

Results

Membrane Insertion Efficiencies of Different Combinations of Shaker TMs. We evaluated the insertion potential of different combinations of segments of the Shaker voltage sensor (the data for the S1–S6, S1–S2, and S5–P–S6 constructs are shown in SI Fig. 9). The N-terminal cytosolic domain of Shaker was deleted to increase the efficiency of *in vitro* translation and translocation, and the reporter protein prolactin (PL) or PL with an artificially generated glycosylation site (PL_{gly}) was fused to the C terminus of the protein (Fig. 1*A*). In all constructs the native glycosylation acceptor sites N259 and N263 in the S1–S2 loop were removed by mutation to Q (30). Instead, the G loop from the human band 3 protein (19) containing a glycosylation acceptor site was inserted into the S3–S4 loop of S1–S4, S1–S3, and S3–S4 to monitor the membrane insertion of S3. These constructs were translated in the absence or presence of dog pancreas rough microsomes (RMs). Aliquots of the translation products obtained in the presence of RMs were further treated by proteinase K to degrade the regions exposed on the cytosolic face of the RMs (Fig. 1*B*). The degree of translocation of the PL reporter across the RM membrane was assayed based on its glycosylation and its resistance against proteinase K.

As shown in Fig. 1*B*, the S1–S4 construct with both the PL and PL_{gly} reporters was efficiently monoglycosylated in the presence of RM (lanes 2 and 5), and no proteinase K-resistant band (lanes 3 and 6) was seen, indicating that the efficiency of membrane integration

Author contributions: L.Z. and N.U. designed research; L.Z., Y.S., and N.U. performed research; L.Z., Y.S., T.H., G.v.H., J.-K.L., I.K., M.S., and N.U. analyzed data; and L.Z., Y.S., and N.U. wrote the paper.

The authors declare no conflict of interest.

This article is a PNAS Direct Submission.

Abbreviations: PL, prolactin; RM, rough microsome; PL_{gly}, PL with an artificially generated glycosylation site; TM, transmembrane; SA, signal anchor.

‖To whom correspondence should be addressed. E-mail: uozumi@biophy.che.tohoku.ac.jp.

This article contains supporting information online at www.pnas.org/cgi/content/full/0611007104/DC1.

BIOCHEMISTRY

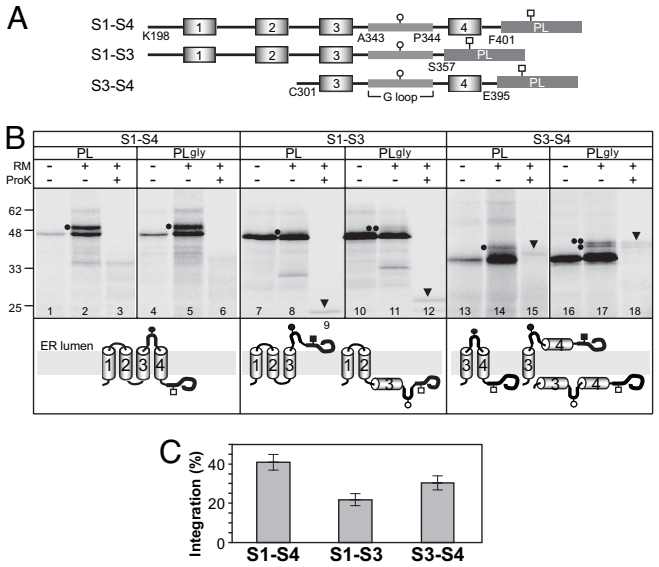

Fig. 1. Membrane insertion efficiencies of different combinations of Shaker TM segments. (*A*) Constructs used to assess the topology of different combinations of S1–S4. The G loop from human band 3 protein (19) containing a glycosylation acceptor site was inserted into the S3–S4 loop, and the reporter protein PL or PL_{gly} was fused to the C terminus of the channel proteins to monitor the membrane insertion of the channel protein. The glycosylation site is shown as circle or square with a bar. (*B*) Assessment of the topology of the constructs shown in *A*. The RNAs were translated in reticulocyte lysate in the absence (−) or presence (+) of RM. After translation, the products were left untreated or were treated with proteinase K (ProK). Single dot, monoglycosylated product; double dots, diglycosylated product; black arrowhead, proteinase K-resistant product. The deduced topologies of the constructs are shown at the bottom of each panel. (*C*) Membrane integration efficiency of the different combinations of TM segments shown in *B*. The percentage integration was calculated as [monoglycosylated and diglycosylated forms × 100/monoglycosylated, diglycosylated, and nonglycosylated forms].

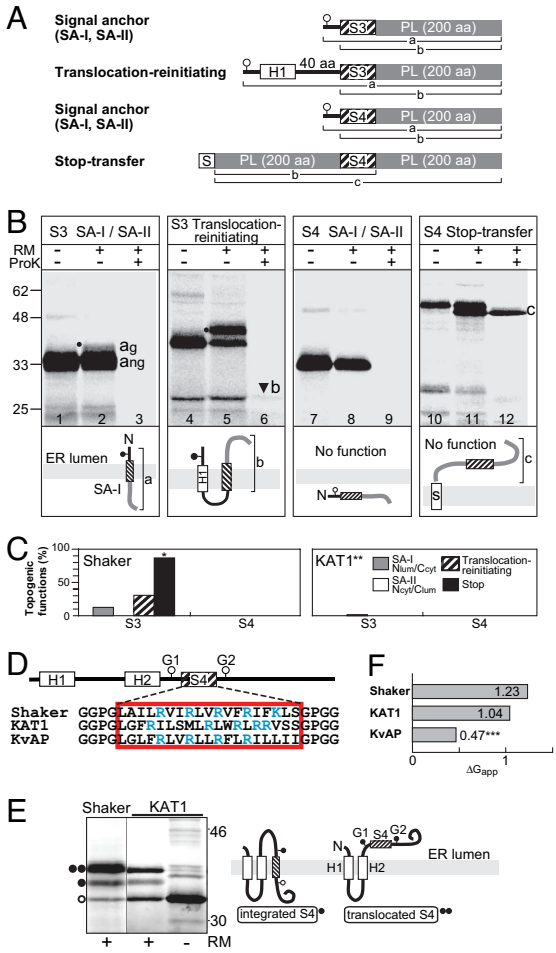

Fig. 2. Topogenic functions of Shaker S3 or S4. (*A*) The model proteins used to assess the topogenic function of S3 or S4 (SA-I, SA-II, translocation-reinitiating function, and stop-transfer function). H1 and S indicate, respectively, the H1 segment and the signal peptide. (*B*) Experimental results and the deduced topologies. a_g, glycosylated product; a_{ng}, nonglycosylated product; b, proteinase K-resistant product; c, proteinase K-resistant product with a cleaved signal peptide. The dots indicate monoglycosylated products. (*C*) Summary of the topogenic functions of Shaker S3 or S4 (*). The results on the stop-transfer function of S3 and the translocation-reinitiating function of S4 are given in *SI Text* (**). The data for KAT1 are from Sato *et al.* (26). The efficiency of topogenic function was calculated using the following formulas: SA-I efficiency = $a_g \times 100/(a_g + a_{ng})$; SA-II efficiency = $b \times k^{-1} \times 100/(a_g + a_{ng})$; translocation-reinitiating efficiency = $b \times k^{-1} \times 100/a_g$; and stop-transfer efficiency = $c \times 100/(b + c)$, where k is the proteinase K protection efficiency of the translocated PL estimated under our experimental conditions using the formula k = (PL after proteinase K treatment)/(PL before proteinase K treatment). The number of [^{35}S]methionines in each digested form was taken into consideration. (*D*) (*Upper*) The model *E. coli* leader peptidase protein has two N-terminal TM segments (H1 and H2) and a large C-terminal domain. S4 from Shaker or KAT1 was inserted into the C-terminal domain at a position where it was flanked by two glycosylation acceptor sites (G1 and G2) (31). (*Lower*) S4 sequences of KvAP, Shaker, and KAT1. GGPG-GPGG flanking sequences were added at the ends of S4 in the model proteins. (*E*) Membrane integration of Shaker and KAT1 S4. (*Left*) Plasmids encoding the constructs were transcribed and translated *in vitro* in the absence (−) and presence (+) of RMs. White circle, nonglycosylated product; single black circle, monoglycosylated product; two black circles, diglycosylated product. (*Right*) If S4 is integrated into the membrane, only G1 will be glycosylated (see left side); if not, both G1 and G2 will be glycosylated (see right side). (*F*) ΔG_{app} values deduced from the data in *E*. The apparent free energy (ΔG_{app}) of S4 insertion is defined as $\Delta G_{app} = -RT \ln(f_{1g}/f_{2g})$, where R is the gas constant, T the absolute temperature, and f_{1g} and f_{2g} are the fractions of monoglycosylated and diglycosylated molecules, respectively. The ΔG_{app} value for KvAP (***) is from Hessa *et al.* (31).

of S1–S4 is comparable to that of the full-length S1–S6 construct (SI Fig. 9). This indicates that the voltage-sensor domain (S1–S4) and the pore domain (S5–P–S6) can integrate independently into the membrane, as seen with KAT1 (24, 26) (SI Fig. 9).

In the case of S1–S3, the PL construct gave rise to a weak monoglycosylated band (Fig. 1*B*, lane 8, and SI Fig. 9*D*, lane 2), and the PL_{gly} construct gave rise to a weak diglycosylated band (Fig. 1*B*, lane 11, and SI Fig. 9*D*, lane 4) in the presence of RM. Both constructs gave rise to a proteinase K-resistant band (lanes 9 and 12). These results indicate that the correct integration of S3 was achieved in a fraction of the molecules, although the integration efficiency was rather low (Fig. 1 *B* and *C*). In KAT1, no integration of S3 is seen in a corresponding construct (26). Because S3 showed efficient membrane integration in the S1–S4 constructs (Fig. 1 *B* and *C* and SI Fig. 9*D*), we conclude that S4 is critical for the membrane integration of S3. Results for the S3–S4 construct indicate that correct integration of S3 and S4 into the membrane occurred in a fraction of the molecules, although the integration efficiency was rather low and some S4 was translocated across the membrane (Fig. 1 *B* and *C*).

Taken together, these results show that Shaker S3 can partially integrate into the membrane in the correct orientation, that S3 in combination with S4 is able to insert into the membrane in the absence of S1 and S2 (albeit with rather low efficiency), and that the isolated S1–S4 domain inserts as efficiently as it does in the context of the full-length protein.

Translocation-Reinitiating Function of Shaker S3 and Lack of Membrane-Inserting Ability of Shaker S4. We next assessed the topogenic activities of Shaker S3 and S4 taken individually (the data

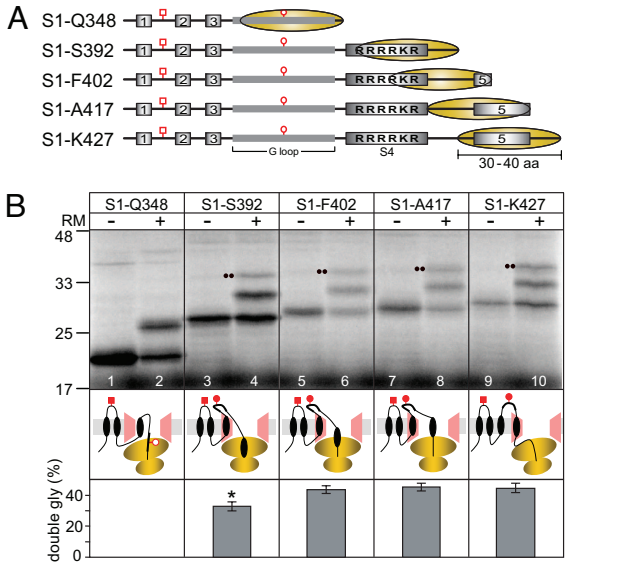

Fig. 3. Sequential integration of Shaker S3–S4 into the membrane. (*A*) Constructs for the translocation intermediates. The native glycosylation acceptor site, N263 (red square), was preserved in the S1–S2 loop to monitor the translocation of S1–S2. The G loop (red circle) was introduced into the S3–S4 loop to monitor the translocation of S3–S4. In the S1–Q348 protein, the glycosylation acceptor site in the S3–S4 loop was positioned inside the ribosome as a control. The position of the ribosome (ellipse) is shown. The distance between ribosomes and the translocon is estimated to be ≈30–40 residues based on the estimation reported by Voss *et al.* (38). (*B*) (*Top* and *Middle*) Assessment of the cotranslational membrane integration of the S3–S4 integration intermediates. Double dots, diglycosylated product. (*Bottom*) Efficiency of membrane integration of S3–S4 in truncated peptides. Efficiency (%) = diglycosylated form × 100/(monoglycosylated form + diglycosylated form). $n = 3$ and $P < 0.05$ (S1–S392 vs. S1–F402, A417, and K427).

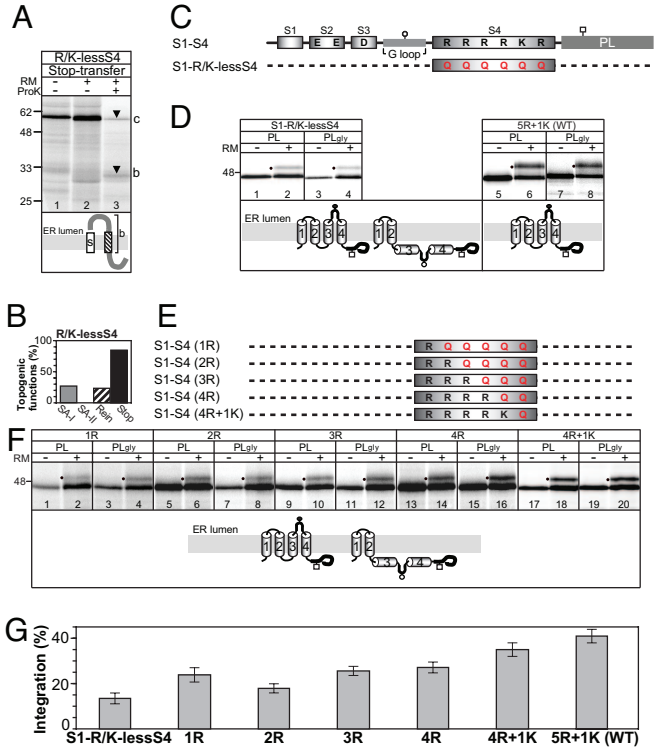

Fig. 4. Cooperative translational integration of Shaker S3–S4 into the membrane. (*A* and *B*) All six conserved positively charged residues (R or K) in S4 in the same S4 model protein as in Fig. 2*A* were replaced by Q (R/K-lessS4) and the SA-I, SA-II, translocation-reinitiating, and stop-transfer functions of the R/K-lessS4 determined in the same manner as in Fig. 2. The data on assessments for SA-I, SA-II, and translocation-reinitiating functions are also shown in SI Fig. 10. (*C* and *D*) Membrane integration of S3–S4 in the S1–S4 construct in which S4 was replaced by R/K-lessS4 to remove the electrostatic interaction between S2/S3 and S4. The efficiency of integration (%) is shown in *G*. (*E* and *F*) Assessment of the contribution of positive charges in S4 to the membrane integration of S3–S4. Increasing numbers of R or K residues were added sequentially to S4 of the S1–R/K-lessS4 construct, starting at the N terminus. The efficiencies of integration are shown in *G*.

for the individual S1, S2, S5, P, and S6 segments are shown in SI Fig. 10). First, a model protein in which S3 or S4 was fused between an N-terminal hydrophilic sequence containing a glycosylation acceptor site and a C-terminal PL reporter molecule was constructed to evaluate the ability of S3 and S4 to mediate membrane insertion with a N_{lum}–C_{cyt} [signal anchor type I (SA-I)] or N_{cyt}–C_{lum} (SA-II) orientation (Fig. 2*A*, first and third lines). For the S3 construct, a weak glycosylated band was seen (Fig. 2 *B*, lane 2, and *C*), indicating that S3 possesses a weak ability to insert into the membrane in the SA-I orientation. Because a proteinase K-protected band was not seen (Fig. 2*B*, lane 3), the isolated Shaker S3 segment is not able to insert into the membrane in the opposite SA-II orientation. With the S4-containing construct, no glycosylated or proteinase K-resistant bands were seen (Fig. 2 *B*, lanes 7–9, and *C*), demonstrating that S4 does not possess any SA function.

Second, because S3 has a N_{cyt}–C_{lum} orientation in the full-length protein, we assessed the activity for initiation of the translocation of S3 alone when the N-terminal region of S3 was placed at the cytosolic side because of the preceding TMs (translocation-reinitiating function) (26, 27). To promote the N_{cyt}–C_{lum} (SA-II) orientation of S3, a SA-I sequence (H1 from *Escherichia coli* leader peptidase) was placed in front of the S3–PL fusion, and a glycosylation acceptor site was engineered in front of the H1 domain to provide a marker for the correct N_{lum}–C_{cyt} orientation of the H1 domain (Fig. 2*A*, second line). Using this construct, low levels of a proteinase K-resistant band were seen (Fig. 2*B*, lane 6), indicating that S3 has the ability to mediate translocation of the following PL sequence into the endoplasmic reticulum lumen, consistent with the results for the S1–S3 constructs shown in Fig. 1. No such translocation-reinitiating activity was seen with KAT1 S3 (26).

Third, we examined whether S4 could stop ongoing translocation and integrate into the membrane as a TM segment with the N_{lum}–C_{cyt} orientation. In this case we used a model protein consisting of a signal peptide, PL, S4, and a second PL (Fig. 2*A*, bottom line). The N-terminal signal peptide targets the model protein to the membrane and is then cleaved off. As shown in Fig. 2*B*, the construct was fully protected from proteinase K (lane 12), indicating that both PL domains were translocated across the RM membrane and hence that S4 lacks stop-transfer function. We conclude that membrane integration of the Shaker S4 segment depends on other segments in the polypeptide chain.

Hessa *et al.* (31) evaluated the membrane-insertion potential of S4 from KvAP (a K_v channel from *Aeropyrum pernix*) by measuring the apparent free energy of the translocon-mediated integration of S4 into the endoplasmic reticulum membrane. To confirm that Shaker and KAT1 S4 lack membrane-insertion properties, we used the same experimental system (31). The core 19 aa of Shaker and KAT1 S4 (shown in the box in Fig. 2*D*) were inserted into the C-terminal domain of *E. coli* leader peptidase between GGPG-GPGG flanking sequences, as in Hessa *et al.* (31). The efficiency of membrane integration of the S4 segments was quantified by SDS/PAGE by measuring the fraction of singly (f_{1g}) and doubly (f_{2g}) glycosylated molecules (Fig. 2*E*). The apparent free energy of S4 insertion was calculated as $\Delta G_{app} = -RT \ln(f_{1g}/f_{2g})$ (see legend for Fig. 2*F*) and was found to be 1.23 kcal/mol for Shaker S4 and 1.04

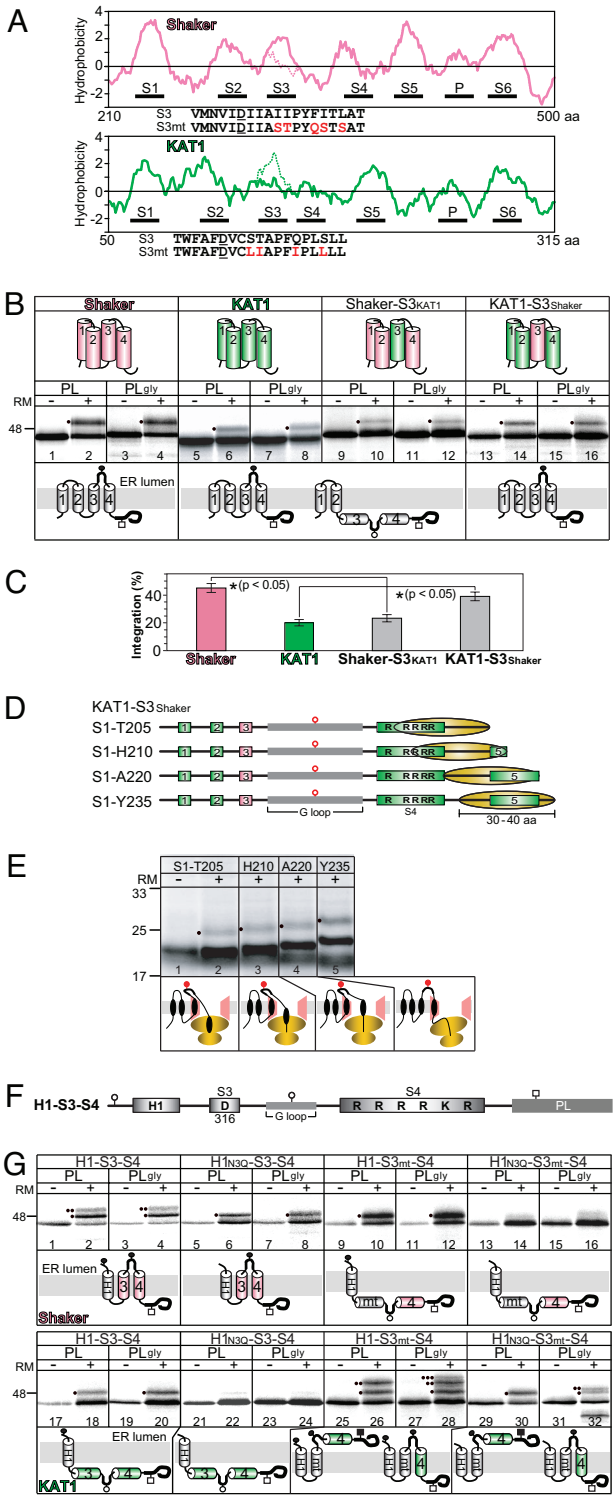

Fig. 5. Effect of the hydrophobicity of S3 in Shaker and KAT1 on membrane integration of S3–S4. (*A*) Hydropathy plots for the wild type and mutants of Shaker and KAT1 generated by the method of Kyte and Doolittle (39) with a window of 13 aa. Shaker S3 and KAT1 S3 in a $H1_{(N3Q)}$–S3–S4 construct were mutated to, respectively, decrease and increase their hydrophobicities in *D* and *E* (dotted line). The mutations are shown in red in the sequences below the traces in *A*. The conserved glutamate (D) is underlined. (*B*) Assessment of membrane integration of the wild-type Shaker and KAT1 and of chimeric proteins based on the construct S1–S4. Shaker-$S3_{KAT1}$ is the Shaker protein containing KAT1 S3, and KAT1-$S3_{Shaker}$ is the KAT1 protein containing Shaker S3. (*C*) Efficiency of membrane integration of S3–S4 in Shaker, KAT1, and the chimeras. Integration (%) = glycosylated form × 100/(glycosylated form + nonglycosylated form). $n = 4$ and $P < 0.05$ for Shaker-$S3_{KAT1}$ vs. KAT1; $n = 4$ and $P < 0.05$ for KAT1-$S3_{Shaker}$ vs. Shaker. (*D*) Constructs for the translocation intermediates KAT1-$S3_{Shaker}$. The G loop (red circle) was introduced into the S3–S4 loop to monitor the translocation of S3–S4. The position of the ribosome (ellipse) is shown. (*E*) Assessment of the cotranslational membrane integration of the S3–S4 integration intermediates of KAT1-$S3_{Shaker}$. (*F*) Model protein for assessing the membrane integration of mutated S3 shown in *A*. H1 was placed in front of S3–S4 as a strong SA-I function. (*G*) Assessment of membrane integration of S3–S4 in the wild-type Shaker and KAT1 the mutated proteins.

kcal/mol for KAT1 (Fig. 2*F*), clearly higher than that of 0.47 kcal/mol for KvAP S4, which is near the threshold for efficient membrane insertion (31). Shaker and KAT1 S4 were therefore significantly less stable in the hydrophobic lipid bilayer, confirming the results shown in Fig. 2 *A–C*.

Sequential vs. Cooperative Membrane Insertion of Shaker S2–S4. The membrane insertion ability of S3 in the S1–S3 construct (Fig. 1) and the translocation-reinitiating function of S3 (Fig. 2) indicate that Shaker S3–S4 insertion may, in part, occur in a sequential or "cotranslational" manner. To test this possibility, mRNAs coding for C-terminal truncated constructs without a stop codon were used (Fig. 3*A*). When the mRNA lacks a stop codon, the synthesized peptide cannot dissociate from the ribosome after being translated and membrane insertion can be monitored for polypeptide chains of different lengths.

Using this approach, we analyzed a series of constructs of different lengths to monitor the insertion of S3–S4 into the membrane. The constructs contained the native N263 glycosylation site in the S1–S2 extracellular loop plus a novel glycosylation site that was generated by insertion of the G-loop sequence into the S3–S4 loop. With the shortest construct, S1–Q348, the glycosylation site in the S3–S4 loop was positioned in the ribosome (Fig. 3*A*) and a monoglycosylated product was seen when the mRNA translated in the presence of RM (Fig. 3*B*, lane 2), indicating that only S1 and S2 were integrated into the membrane. Using construct S1–S392, in which the glycosylation site in the S3–S4 loop was placed far enough from the ribosome to be glycosylated but S4 was still within in the ribosome (Fig. 3*A*), a diglycosylated product was seen (Fig. 3*B*, lane 4), showing that S3 can at least to some extent insert cotranslationally into the membrane without the assistance of S4, in contrast to the S3 from KAT1 (26). The amount of membrane-inserted S3–S4 increased further with increasing polypeptide length, suggesting that interactions between S3 and S4 enhance the integration efficiency (cooperative or posttranslational insertion).

Based on the results of S3–S4 insertion presented so far (Figs. 1 and 3), we predicted that interactions among charged residues in S2, S3, and S4 might be critical for the membrane integration of S3–S4, as seen for KAT1 (26). We evaluated this possibility by converting all of the positively charged residues in S4 into glutamine residues (Q) to eliminate electrostatic interaction among charged residues in S2, S3, and S4 and to increase the hydrophobicity of S4. S4 lacking R/K (R/K-lessS4) was found to have strong stop-transfer function (Fig. 4 *A–C*), in stark contrast to the lack of stop-transfer function of wild-type S4 (Fig. 2 *A–C*). Nevertheless, the S1–R/K-lessS4 construct integrated less efficiently into the membrane than wild-type S1–S4 (5R + 1K) (Fig. 4 *D* and *G*).

We designed a further series of constructs in which an increasing number of R/K residues was introduced, starting at the N terminus of S4 (1R, 2R, 3R, 4R, and 4R + 1K) (Fig. 4*E*). As shown in Fig. 4 *F* and *G*, the intensity of the glycosylated band increased with increasing number of positively charged residues in the construct (Fig. 4 *E* and *G*). We conclude that positively charged residues in S4 promote the cooperative, posttranslational insertion of the Shaker voltage-sensor domain.

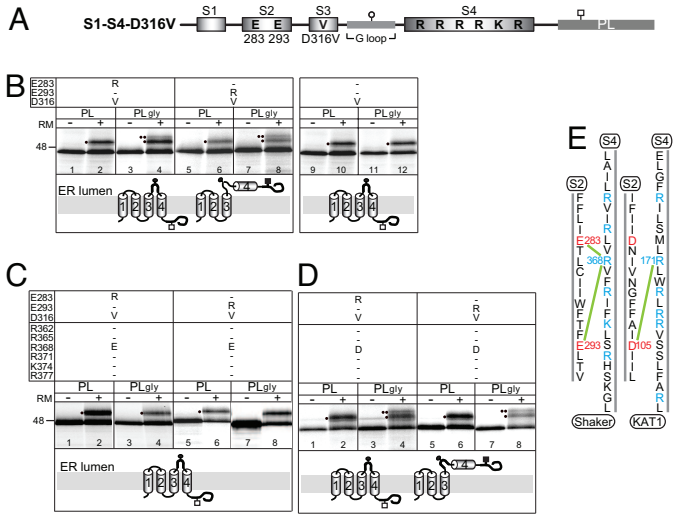

Fig. 6. Identification of the paired residues involved in the electrostatic interactions between S2 and S4. (*A*) Models of S1–S4 constructs containing D316V for charged reverse mutations at E283 or E293 in S2 and R368 in S4. (*B–D*) Assessment of membrane integration of the mutants. (*E*) Salt bridge formation between E283 or E293 and R368 during membrane topogenesis of the voltage sensor in Shaker (*Left*). The electrostatic interaction between D141 and R171 in KAT1 reported previously (26, 27) is shown in *Right*. The green lines indicate salt bridges.

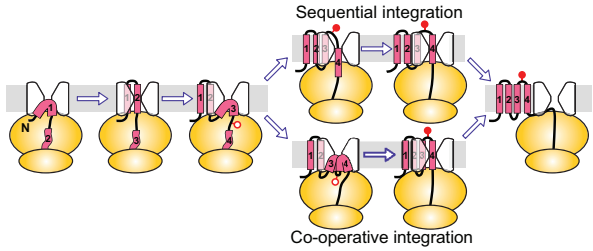

Fig. 7. Model of the membrane integration of the voltage sensor. S1–S2 is inserted sequentially into the membrane, and then the following S3–S4 is inserted into the membrane via two pathways: (*i*) S3–S4 is inserted in a sequential, cotranslational manner. (*ii*) S3–S4 is synergistically inserted in a cooperative, posttranslational manner and remains in the membrane by electrostatic interactions among S2, S3, and S4.

Effect of the Hydrophobicity of S3 on the Sequential Integration of Shaker S3–S4. Comparison of the hydrophobicity of all segments between Shaker and KAT1 indicates that a main difference is that Shaker S3 and S4 are more hydrophobic than KAT1 S3 and S4 (Fig. 5*A* and SI Fig. 8). In contrast to Shaker, isolated KAT1 S3 shows no membrane integration (26, 27), prompting us to study the role of hydrophobicity further.

Various chimeras of Shaker and KAT1 were constructed by swapping the S3 segments. As shown in Fig. 5 *B* and *C*, the KAT1-S3$_{Shaker}$ chimera (Shaker S3 inserted into KAT1 S1–S4) showed an increase in the intensity of the glycosylated band to a value comparable to that of wild-type Shaker S1–S4, whereas the Shaker-S3$_{KAT1}$ chimera (KAT1 S3 in Shaker S1–S4) showed a decrease in glycosylation efficiency to a value similar to that of wild-type KAT1 S1–S4. These results indicate that the higher hydrophobicity of Shaker S3 favors sequential insertion of Shaker S3–S4.

We also examined the membrane insertion of these constructs using truncated mRNAs. Unlike the wild-type KAT1 (26), the constructs S1–T205 and S1–H210 of KAT1-S3$_{Shaker}$ chimera showed glycosylated bands, indicating that S3 had been partially inserted into the membrane even though S4 had not emerged from the ribosome (Fig. 5 *D* and *E*).

To further clarify the effect of the hydrophobicity of S3 on S3–S4 integration, we used H1$_{(N3Q)}$–S3–S4–PL$_{(gly)}$ constructs (Fig. 5*F*). In these constructs, S2 was eliminated from the model protein to remove the assistance to S3–S4 insertion provided by the negatively charged residues in S2 (see below). A diglycosylated band was seen with Shaker H1–S3–S4–PL$_{(gly)}$ (Fig. 5*G*, lanes 1–4), but not with KAT1 H1–S3–S4–PL$_{(gly)}$ (lanes 17–20). The diglycosylated band for the Shaker construct and the monoglycosylated band for the KAT1 construct were not seen when the glycosylation site at the N terminus was removed (H1$_{N3Q}$–S3–S4–PL$_{(gly)}$), confirming that H1 was inserted into the membrane (lanes 5–8 and 21–24). These results show that Shaker S3, but not KAT1 S3, can help S4 integrate into the membrane. When the hydrophobicity of Shaker S3 was decreased to be similar to that of KAT1 S3 by the introduction of several mutations (see Fig. 5*A*, mutated residues shown in red), no membrane insertion of Shaker S3–S4 was seen (Fig. 5*G*, lanes 9–16), as with wild-type KAT1 (lanes 17–24). In contrast, on increasing the hydrophobicity of KAT1 S3 toward that of Shaker S3 by mutation, S3–S4 acquired membrane integration ability (lanes 25–32), as with wild-type Shaker (lanes 1–8). A triglycosylated band was also seen with H1–S3$_{mt}$–S4–PL$_{gly}$ (Fig. 5*G*, lane 28), and a diglycosylated band was seen with H1$_{N3Q}$–S3$_{mt}$–S4–PL$_{gly}$ (lane 32), indicating that S4 was released into the endoplasmic reticulum lumen in a fraction of the molecules.

These results suggest that relatively hydrophobic S3 segments, such as Shaker S3, are likely to have the ability to mediate sequential S3–S4 membrane integration, whereas in KAT1 the S1 and/or S2 segments are also required and insertion is cooperative.

Specific Electrostatic Interactions Between E283 or E293 in S2 and R368 in S4 During Membrane Topogenesis. In KAT1, electrostatic interactions between charged residues in S2 and S4 promote membrane integration of S3–S4 (26, 27). We constructed a series of charge-reversal mutations in Shaker H1$_{(N3Q)}$–S3–S4 in an attempt to identify charge pairs formed between D316 in S3 and positively charged residues in S4, but we failed to do so (data not shown). On the assumption that D316 might interfere with the identification of electrostatic interactions between E283 or E293 in S2 and positively charged residues in S4, we next used mutants in which D316 was changed to V to simplify the further analysis (Fig. 6 and SI Fig. 11). Mutation of E282 or E293 in S2 to R (E283R/D316V or E293R/D316V) resulted in a diglycosylated band (Fig. 6*B*, lanes 4 and 8), indicating that these mutant S2 segments could not retain S4 into the membrane, but caused its release into the lumen of the RMs. We reasoned that, if the loss of electrostatic interactions is responsible for this effect, the membrane insertion of S4 might be rescued by a second reverse mutation of R to E in S4. Among the screened constructs (Fig. 6*C* and SI Fig. 11), two reversal mutants, E283R/D316V/R368E (Fig. 6*C*, lanes 1–4) and E293R/D316V/R368E (lanes 5–8), gave a monoglycosylated band, similar to the original D316V construct (Fig. 6*B*, lanes 9–12). These results imply that electrostatic interactions help to retain S4 in the membrane.

To verify the structure-specific pairing between E283 or E293 and R368, R368 was replaced by D (instead of E) in the reversal mutants, because aspartate has the same charge as glutamate but a side chain that is shorter by one C—C bond (≈1.53 Å) (Fig. 6*D*). The resulting proteins gave rise to a diglycosylated band, implying a loss of the electrostatic interaction (Fig. 6*D*, lanes 4 and 8). Thus, the electrostatic interactions between E283 or E293 in S2 and R368 in S4 are strictly constrained by side-chain length. Salt bridges are formed between opposite charged residues that are closer than 4 Å (32). E283 or E293 in S2 is therefore likely to be adjacent to R368 in S4 and to form salt bridges during biogenesis (Fig. 6*E*). The

formation of a charge pair between E293 and R368 during biogenesis is consistent with the corresponding electrostatic interactions between D105 in S2 and R171 in S4 reported in our previous study on KAT1 topogenesis (26, 27) (Fig. 6*E*).

Discussion

Our study on the membrane topogenesis of Shaker suggests that cooperative (posttranslational) integration of the voltage-sensor TM segments is a property common to K_v channels and that a combination of hydrophobic and electrostatic forces involving S2, S3, and S4 controls the membrane insertion of the voltage sensor.

Because Shaker S3 has a higher hydrophobicity than KAT1 S3 (Fig. 5*A* and SI Fig. 8), we predicted that, in contrast to KAT1 S3, it might be able to insert by itself into the membrane and subsequently help pull S4 into the membrane. As predicted, membrane integration of S3 without S4 was observed (Figs. 1 and 2), and sequential (cotranslational) integration of the isolated S3–S4 part was also seen (Figs. 1 and 3). In contrast, little integration of S3 and S3–S4 was seen with KAT1 (26). Thus, unlike KAT1, cotranslational membrane integration of the isolated Shaker S3 segment and the S3–S4 "helical hairpin" is possible in the absence of other parts of the voltage-sensor domain. Examination of the effects of changes in S3 hydrophobicity on the membrane insertion of S3–S4 (Fig. 5) demonstrates that the insertion ability of Shaker S3 results from its higher hydrophobicity.

On the other hand, Shaker S3 requires the presence of S4 for fully efficient membrane integration (Fig. 1), and the membrane-unstable S4 needs the preceding S1–S3 TMs (Figs. 1 and 2). Removal of charged residues in S4 significantly decreases the membrane integration of S3–S4 (Fig. 4). In the context of the full S1–S4 voltage-sensor domain, the membrane insertion efficiency of S3–S4 decreased when E283 and/or E293 in S2 were neutralized, likely destroying the electrostatic interactions between S2 and S4 (SI Fig. 12). Finally, the efficiency of S3 integration increased when S4 was exposed from the ribosome, compared with a situation where S4 were masked by the ribosome (Fig. 3). These results suggest that the Shaker voltage-sensor domain integrates into the endoplasmic reticulum membrane in a partly cooperative fashion and that electrostatic interactions among S2, S3, and S4 are critical for membrane integration. Taking into consideration the results of our previous study on KAT1 (26) and the present study on Shaker, we predict that cooperative, posttranslational integration of the voltage-sensor domain will be a property common to all K_v channels and that electrostatic interactions among S2, S3, and S4 are important for the process.

The crystal structure of a closed form of the Sec 61 translocon has revealed that the "pore ring" is only 5–8 Å in diameter (33). If the active, open form of the translocon can accommodate two or more α-helices at a time, it is possible that the nascent S3 and S4 helices enter the translocon together. The critical electrostatic interactions between E283 and/or E293 in S2 and R368 in S4 (Fig. 6) suggest the close proximity of E283 or E293 and R368 during biogenesis. Presumably, after S2 exits the translocon, it remains close enough to the nascent chain in the translocation channel to be able to interact with the S3–S4 part (Fig. 7).

Our data fit the current picture of K_v channel structure. In electrophysiological measurements on Shaker, charge pairs formed between E283 in S2 and R368 or R371 in S4 and between E293 in S2 or D316 in S3 and K374 in S4 have been suggested to form an electrostatic interaction network that stabilizes the structure of the channel (34, 35). A further study revealed that the interaction between Shaker E283 and R368 occurs at the resting membrane potential, whereas that between E283 and R371 occurs in the activated conformation (36, 37). A recent structural model also shows E293 interacting with R368 in the resting conformation (7). The crystal structure of $K_v1.2$ in the open conformation shows that residues corresponding to R368 and R371 in Shaker face the S1 and S2 helices, where they make salt bridges with as yet unidentified acidic residues (11). Thus, electrostatic interactions play a critical role not only in stabilizing the voltage sensor in the intact protein but also during the process of membrane integration.

Materials and Methods

Plasmid Constructions. The DNA encoding the Shaker B channel was provided by Lily Y. Jan (29). For the topological assay, DNA encoding S1–S2 (K198–D310), S1–S3 (K198–S357), S1–S4 (K198–F401), S1–S6 (K198–N500), S3–S4 (C301–E395), or S5–P–S6 (Q383–N500) was fused to the reporter PL gene with or without the N-glycosylation acceptor sequence (PL or PL_{gly}) in the pCITE-2a vector (Novagen, Madison, WI). In glycosylation mapping, a glycosylation site, NSS, was inserted into different positions in the S3–S4 loop.

***In Vitro* Transcription, Translation, and Translocation.** The plasmids were linearized by ScaI and transcribed *in vitro* at 37°C for 1 h by using T7 RNA polymerase under standard conditions. The mRNAs were translated for 1 h at 30°C in the reticulocyte lysate system *in vitro* in the absence or presence of dog pancreas RM membranes. [^{35}S]Methionine was used to label the proteins. After translation, for the protease protection assay, the products were incubated on ice for 40 min in the presence of proteinase K, the protease was inactivated by trichloroacetic acid precipitation, and the products were separated on SDS/PAGE gels, which were subjected to autoradiography.

This work was supported by grants-in-aid for scientific research (Grants 19380058 and 17078005 to N.U.) and postdoctoral fellowships (to Y.S.) from the Ministry of Education, Culture, Sports, Science and Technology of Japan and the Japan Society for the Promotion of Science.

1. MacKinnon R (2003) *FEBS Lett* 555:62–65.
2. Cha A, Snyder GE, Selvin PR, Bezanilla F (1999) *Nature* 402:809–813.
3. Glauner KS, Mannuzzu LM, Gandhi CS, Isacoff EY (1999) *Nature* 402:813–817.
4. Laine M, Lin MC, Bannister JP, Silverman WR, Mock AF, Roux B, Papazian DM (2003) *Neuron* 39:467–481.
5. Cuello LG, Cortes DM, Perozo E (2004) *Science* 306:491–495.
6. Aggarwal SK, MacKinnon R (1996) *Neuron* 16:1169–1177.
7. Durell SR, Shrivastava IH, Guy HR (2004) *Biophys J* 87:2116–2130.
8. Shrivastava IH, Durell SR, Guy HR (2004) *Biophys J* 87:2255–2270.
9. Tombola F, Pathak MM, Isacoff EY (2005) *Neuron* 45:379–388.
10. Yellen G (2002) *Nature* 419:35–42.
11. Long SB, Campbell EB, Mackinnon R (2005) *Science* 309:897–903.
12. Long SB, Campbell EB, Mackinnon R (2005) *Science* 309:903–908.
13. Jiang Y, Lee A, Chen J, Ruta V, Cadene M, Chait BT, MacKinnon R (2003) *Nature* 423:33–41.
14. Jiang Y, Ruta V, Chen J, Lee A, MacKinnon R (2003) *Nature* 423:42–48.
15. Rapoport TA, Goder V, Heinrich SU, Matlack KE (2004) *Trends Cell Biol* 14:568–575.
16. White SH, von Heijne G (2005) *Curr Opin Struct Biol* 15:378–386.
17. Rothman RE, Andrews DW, Calayag MC, Lingappa VR (1988) *J Biol Chem* 263:10470–10480.
18. Lu Y, Xiong X, Helm A, Kimani K, Bragin A, Skach WR (1998) *J Biol Chem* 273:568–576.
19. Ota K, Sakaguchi M, Hamasaki N, Mihara K (1998) *J Biol Chem* 273:28286–28291.
20. Johansson M, von Heijne G (1996) *J Biol Chem* 271:25912–25915.
21. Uozumi N, Nakamura T, Schroeder JI, Muto S (1998) *Proc Natl Acad Sci USA* 95:9773–9778.
22. Tu L, Wang J, Helm A, Skach WR, Deutsch C (2000) *Biochemistry* 39:824–836.
23. Lu J, Deutsch C (2005) *Biochemistry* 44:8230–8243.
24. Umigai N, Sato Y, Mizutani A, Utsumi T, Sakaguchi M, Uozumi N (2003) *J Biol Chem* 278:40373–40384.
25. Shih TM, Goldin AL (1997) *J Cell Biol* 136:1037–1045.
26. Sato Y, Sakaguchi M, Goshima S, Nakamura T, Uozumi N (2002) *Proc Natl Acad Sci USA* 99:60–65.
27. Sato Y, Sakaguchi M, Goshima S, Nakamura T, Uozumi N (2003) *J Biol Chem* 278:13227–13234.
28. Jan LY, Jan YN (1990) *Nature* 345:672.
29. Tempel BL, Papazian DM, Schwarz TL, Jan YN, Jan LY (1987) *Science* 237:770–775.
30. Santacruz-Toloza L, Huang Y, John SA, Papazian DM (1994) *Biochemistry* 33:5607–5613.
31. Hessa T, White SH, von Heijne G (2005) *Science* 307:1427.
32. Barlow DJ, Thornton JM (1983) *J Mol Biol* 168:867–885.
33. Van den Berg B, Clemons WM, Jr, Collinson I, Modis Y, Hartmann E, Harrison SC, Rapoport TA (2004) *Nature* 427:36–44.
34. Papazian DM, Shao XM, Seoh SA, Mock AF, Huang Y, Wainstock DH (1995) *Neuron* 14:1293–1301.
35. Tiwari-Woodruff SK, Schulteis CT, Mock AF, Papazian DM (1997) *Biophys J* 72:1489–1500.
36. Tiwari-Woodruff SK, Lin MA, Schulteis CT, Papazian DM (2000) *J Gen Physiol* 115:123–138.
37. Seoh SA, Sigg D, Papazian DM, Bezanilla F (1996) *Neuron* 16:1159–1167.
38. Voss NR, Gerstein M, Steitz TA, Moore PB (2006) *J Mol Biol* 360:893–906.
39. Kyte J, Doolittle RF (1982) *J Mol Biol* 157:105–132.